Journal of Power Sources 196 (2011) 9246–9253

Contents lists available at ScienceDirect

Journal of Power Sources

journal homepage: www.elsevier.com/locate/jpowsour

Study on proton-conducting solid oxide fuel cells with a conventional nickel cermet anode operating on dimethyl ether

Yu Liu [a], Youmin Guo [a], Wei Wang [a], Chao Su [a], Ran Ran [a], Huanting Wang [b], Zongping Shao [a,b,*]

[a] State Key Laboratory of Materials-Oriented Chemical Engineering, Nanjing University of Technology, No. 5 Xin Mofan Road, Nanjing 210009, PR China
[b] Department of Chemical Engineering, Monash University, Clayton, VIC 3800, Australia

ARTICLE INFO

Article history:
Received 25 June 2011
Received in revised form 15 July 2011
Accepted 16 July 2011
Available online 22 July 2011

Keywords:
Dimethyl ether
Proton conductor
Solid oxide fuel cells
Coke formation
Steam reforming

ABSTRACT

This study investigates dimethyl ether (DME) as a potential fuel for proton-conducting SOFCs with a conventional nickel cermet anode and a $BaZr_{0.4}Ce_{0.4}Y_{0.2}O_{3-\delta}$ (BZCY4) electrolyte. A catalytic test demonstrates that the sintered Ni + BZCY4 anode has an acceptable catalytic activity for the decomposition and steam reforming of DME with CO, CH_4 and CO_2 as the only gaseous carbon-containing products. An O_2-TPO analysis demonstrates the presence of a large amount of coke formation over the anode catalyst when operating on pure DME, which is effectively suppressed by introducing steam into the fuel gas. The selectivity towards CH_4 is also obviously reduced. Peak power densities of 252, 280 and 374 mW cm^{-2} are achieved for the cells operating on pure DME, a DME + H_2O gas mixture (1:3) and hydrogen at 700 °C, respectively. After the test, the cell operating on pure DME is seriously cracked whereas the cell operating on DME + H_2O maintains its original integrity. A lower power output is obtained for the cell operating on DME + H_2O than on H_2 at low temperature, which is mainly due to the increased electrode polarization resistance. The selection of a better proton-conducting phase in the anode is critical to further increase the cell power output.

1. Introduction

Fuel flexibility is one of the most significant advantages of solid oxide fuel cells (SOFCs) over polymer electrolyte membrane fuel cells (PEMFCs). Because of a high operating temperature, even a nickel catalyst shows fast electrode kinetics. As a result, in addition to hydrogen, many fuels, such as hydrocarbons, ammonia and carbon monoxide, can be directly oxidized over a nickel-based SOFCs anode [1–5]. This feature is highly attractive because hydrocarbons and other fuels are much easier to be find, store and transport than hydrogen.

Conventional SOFCs use oxygen ion-conducting oxides [6,7], including stabilized zirconia and doped ceria, as the electrolytes, and the fuels react with oxygen ions transported from the cathode side with the formation of H_2O and CO_2 as the final products in the anode chamber, which may dilute the fuel gas and reduce efficiency. Recently, SOFCs with proton-conducting oxides as the electrolytes have received increasing attention [8–10]. In 1981, Iwahara et al. first observed that some perovskite oxides had proton conductivity at high temperatures [11]. Because the size of a proton is much smaller than that of an oxygen ion, it is believed that high conductivity is easier to achieve in proton conductors than in oxygen ion conductors at lower temperatures. Indeed, selected $BaCe_{0.8-x}Zr_xY_{0.2}O_{3-\delta}$-based proton conductors show comparable conductivity at intermediate temperatures to that of doped ceria and $La_{1-x}Sr_xGa_{0.8}Mg_{0.2}O_{3-\delta}$ (LSGM) [12,13], which are the oxygen ion conductors with the highest known oxygen ion conductivity [14,15]. Increasing numbers of scientific papers about proton-conducting SOFCs have recently appeared in the literature. However, in those studies, attention was mainly paid to the new electrolytes or cathodes, and there have been few studies examining different fuels.

Dimethyl ether (DME) is the simplest ether and has physical properties that are similar to those of liquefied petroleum gases (LPGs) [16]. For example, DME is a gas at room temperature and ambient pressure, but it can be easily liquefied at medium pressure (1.35 MPa) at room temperature. All of the available infrastructure for LPG can be used for DME. Therefore, the storage and transportation of DME is relatively easy. In addition, natural gas, coal and biomass can also act as raw materials for DME synthesis, and, with advances in the synthetic technique, DME may be widely available in the near future. Recently, the use of DME as a fuel for SOFCs has received attention [17–21]. Because of the high energy density of liquid DME, DME-fueled SOFCs have great potential for portable or domestic uses. Previously, we studied oxygen ion-conducting SOFCs operating on DME [20,21]. Coke formation can occur with pure DME as the fuel [20]; however, through internal partial oxidation under the catalysis of nickel cermet anode,

* Corresponding author. Tel.: +86 25 83172256; fax: +86 25 8317224.
E-mail addresses: zongping.shao@monash.edu, shaozp@njut.edu.cn (Z. Shao).

0378-7753/$ – see front matter © 2011 Elsevier B.V. All rights reserved.
doi:10.1016/j.jpowsour.2011.07.051

promising cell performance was achieved with reduced coke formation [21]. Up until now, the application of hydrocarbon or oxygenated-hydrocarbon as a fuel of proton-conducting SOFCs has seldom been reported [22–24]. In proton-conducting SOFCs, the electrochemical oxidation of fuel occurs only at the cathode side; therefore, the hydrocarbons should first be converted to hydrogen, which is the only possible direct fuel for proton-conducting SOFCs. Internal steam reforming may be preferable to internal partial oxidation because it can maximize hydrogen production. In addition, the endothermic reaction of steam reformation can consume the partial heat produced during exothermic fuel electrochemical oxidation over the cathode, thereby increasing the overall energy efficiency.

In this study, we report an investigation of DME as a fuel of anode-supported proton-conducting SOFCs with a conventional nickel cermet anode. A sintered Ni + $BaZr_{0.4}Ce_{0.4}Y_{0.2}O_{3-\delta}$ (Ni + BZCY4) cermet anode was applied as the catalyst and the internal steam reformation of DME at intermediate temperatures was attempted. This study examined coke formation over the anode, cell integrity and cell performance at different DME-to-H_2O ratios. A comparative study with hydrogen as fuel was also performed.

2. Experimental materials and methods

2.1. Fuel cell fabrication

The fuel cells used in this study were anode-supported, thin-film, electrolyte proton-conducting SOFCs with a Ni + BZCY4 anode, a BZCY4 electrolyte, and a $Ba_{0.5}Sr_{0.5}Co_{0.8}Fe_{0.2}O_{3-\delta}$ (BSCF) cathode. BZCY4 was prepared using a complexing sol–gel method. Detailed information about the preparation can be found in our previous publication [25]. The BZCY4 powder was calcined at 1000 °C for 10 h in air for later use in the proton-conducting phase of the anode or the electrolyte. To fabricate the fuel cell, the as-prepared BZCY4 powder and commercial NiO (Chengdu Shudu Nano-Science Co., Ltd.) were co-milled at a weight ratio of 40:60 by high energy ball milling (Pulverisette 6) using ethanol as a solvent to reach the desired particle size. Polyvinyl butyral (PVB, molecular weight 30,000–45,000) was also added to the NiO + BZCY4 mixture as a pore-former during the ball milling process. After ball milling at 400 rpm for 30 min, the obtained slurry was dried in an electric oven and prepared into disk-shape anode substrate by dry pressing under a hydraulic pressure of 150 MPa using a stainless steel die. After cleaning the surface of the anode substrate within the die by air brushing, a suitable amount of fluffy BZCY4 powder with ultralow packing density was carefully and homogeneously distributed onto the entire exposed anode surface. The electrolyte and the anode were co-pressed again under a pressure of 300 MPa for 2 min. After slowly being released from the die, the dual layer cells were sintered at 1450 °C in air for 5 h to create a dense BZCY4 thin-film electrolyte on the anode substrate. The BSCF powder was prepared by the same complexing sol–gel method of BZCY4. To fabricate the cathode layer, BSCF powder was mixed with a solution of ethylene glycol and isopropanol by using high-energy ball milling, and the slurry was subsequently painted onto the central surface of the sintered BZCY4 surface with a geometric surface area of 0.48 cm^2. The cells were then fired at 1000 °C for 2 h in air to obtain single cells for later use.

2.2. Catalytic testing

The catalytic activity of the anode material for DME decomposition and the steam reforming reactions was evaluated in a fixed-bed catalytic reactor. A feed gas of DME, DME + He or DME + He + H_2O was introduced to the reaction section in which an 8 mm diameter quartz reactor was mounted vertically inside a tubular electric furnace. Before the test, the NiO + BZCY4 (60:40 by weight) material was sintered at 1450 °C in air for 5 h to make the properties as similar as possible to the real anode. Samples of 40–60 mesh were used for all tests. Approximately 0.2 g NiO + BZCY4 catalysts were diluted with silica sand to avoid temperature gradients and then loaded in the quartz reactor. The reactor was heated by an electric furnace to 750 °C, and hydrogen was introduced at a flow rate of 80 ml min^{-1} [STP] to allow the reduction of nickel oxide in the anode catalyst to metallic nickel. After reduction for approximately 1 h, the gas was switched to a mixture of DME + He or DME + He + H_2O with fixed DME and He flow rates of 10 and 80 ml min^{-1} [STP], respectively, which were precisely controlled by digital mass flow controllers. After the reactions, the effluent from the reactor was transferred into the analysis section, which consisted of an online Varian 3800 GC equipped with Hayesep Q, Poraplot Q, 5 Å molecular sieve capillary columns, a thermal conductivity detector (TCD) and a flame ionization detector (FID) for gas composition analysis. The tested temperatures were ranged from 750 to 450 °C at 50 °C per step. DME-to-H_2O molar ratios of 1:1, 1:2 and 1:3 were tested. The water was introduced by a constant flow pump (Wufeng, LC-P100 Pump). The conversion of DME was mainly calculated taking into account the amount of DME consumed. In certain cases, it was also determined on the basis of the H and C contents of the reactant and products. Selectivities towards hydrogen and different products were calculated based on the equation in the published paper [26].

2.3. Characterization

For the carbon deposition tests, the NiO + BZCY4 catalysts were first sintered at 1450 °C for 5 h. The sintered catalysts with a 40–60 mesh were placed in a flow-through-type quartz tube reactor and reduced by hydrogen at 700 °C for 1 h. Next, DME or DME + H_2O at different DME-to-H_2O ratios were introduced into the reactor at 700 °C for 30 min, and the DME flow rate was maintained at 40 ml min^{-1} [STP]. The treated samples were quickly cooled to room temperature under the protection of a helium atmosphere to perform a subsequent oxygen temperature-programmed oxidation (O_2-TPO) experiment to characterize the eventual carbon deposits formed. Approximately 0.02 g catalysts were introduced into a U-shaped quartz reactor with a 4 mm inner diameter. A gas mixture containing 10 vol.% O_2 in Ar (10 vol.% O_2–Ar, 15 ml min^{-1} [STP]) was passed through the sample, which was heated from room temperature to 850 °C at a constant rate of 10 °C min^{-1}. The deposited solid carbon on the Ni + BZCY4 surface was then progressively oxidized to CO_2. The analysis of the gases was performed continuously with an on-line mass spectrometer (Hiden, QIC-20MS).

The evaluation of cell performance was performed in an in-lab-constructed SOFC test station equipped with a Keithley 2420 source meter. The anode side of the cells was sealed with Ag paste. During the measurement, hydrogen (humidified by bubbling water at room temperature), pure DME, or a mixture of DME + H_2O (1:3) was flowed into the anode chamber at the flow rate of 80 ml min^{-1} [STP], and the cathode was exposed to ambient air. The NiO in the anode was reduced *in situ* to metallic Ni by hydrogen. The current–voltage characteristics of the single cells were determined by linear sweep voltammetry at intervals of 50 °C over a temperature range of 700–500 °C. Electrode performance was also determined based on the complete cells configuration, and the electrochemical impedance spectroscopy (EIS) of the cells under different fuels was measured under open circuit voltage (OCV) conditions using a Solartron 1260 Frequency Response Analyzer combined with a Solartron 1287 Potentiostat. The frequency ranged from 0.1 to 1000 kHz, and the signal amplitude was 10 mV. After testing, the microstructure and cross-sectional morphologies

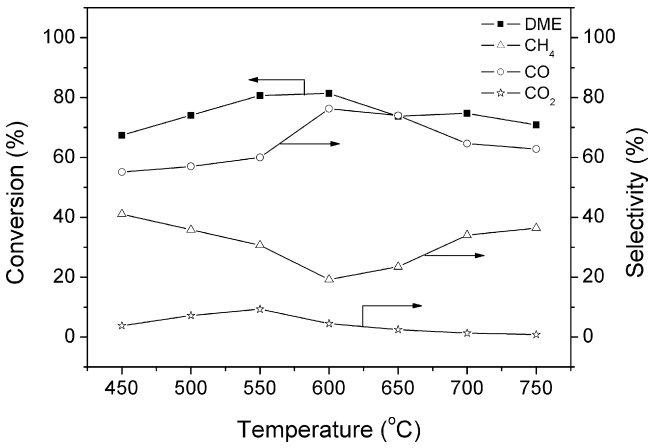

Fig. 1. DME conversion and products selectivity over the Ni + BZCY4 catalyst at various temperatures.

of the tested cells were investigated with an environmental scanning electron microscope (ESEM, Model QUANTA-200).

3. Results and discussion

3.1. Catalytic performance

We first investigated the catalytic activity of the Ni + BZCY4 anode for a DME decomposition reaction, which is similar to the non-catalytic homogeneous cracking CH_4, CO and CO_2 were found to be the only detectable carbon-containing gaseous species in the effluent gas from the catalytic decomposition. Fig. 1 shows the DME conversion and the CH_4, CO and CO_2 selectivity for DME over the Ni + BZCY4 catalyst at various temperatures. In a previous study, we demonstrated that DME conversion by thermal decomposition is relatively low at less than 25% even at 850 °C [20]. In this study, approximately 68% of DME was already decomposed at 450 °C by catalytic decomposition with CH_4 and CO as the main carbon-containing products, and the amount of CO_2 was quite low. This suggests that the main reaction for the catalytic reaction over the Ni + BZCY4 catalyst is $CH_3OCH_3 \rightarrow CH_4 + H_2 + CO$. However, the higher selectivity of CO than CH_4 implies that coke formation was likely to occur over the Ni + BZCY4 catalyst. The possible carbon deposition over Ni + BZCY4 is discussed later in detail. It is very interesting that the DME conversions were all within the range of 67–81% between 450 and 750 °C with the maximum conversion being reached at 600 °C. At the same temperature, CH_4 selectivity also reached a minimum of approximately 20%. This finding is different for the case of Ni + YSZ as the catalyst for which an increase in DME conversion with temperatures between 600 and 750 °C was observed [20]. Clearly, the large difference in catalytic activity between the Ni + YSZ and Ni + BZCY4 catalysts for DME decomposition originated from the difference in the ion-conducting phase within the catalysts.

Because hydrogen is the only possible direct fuel that can be oxidized in proton-conducting SOFCs, it is preferable that DME be converted to hydrogen with maximum selectivity. It was reported that some catalysts have high catalytic activity for DME steam reforming [27–31], and DME conversion as high as 100% and H_2 selectivity higher than 90% were reported at a temperature of approximately 350 °C over a Cu spinel and a solid-acid composite catalyst [32]. The performance of Ni + BZCY4 as a catalyst for DME steam reforming was further investigated. It was found that CH_4, CO_2 and CO remained the main carbon-containing products when introducing steam into DME fuel gas. Fig. 2(a)–(c) shows the DME conversion, CH_4, CO_2 and CO selectivity over Ni + BZCY4 at

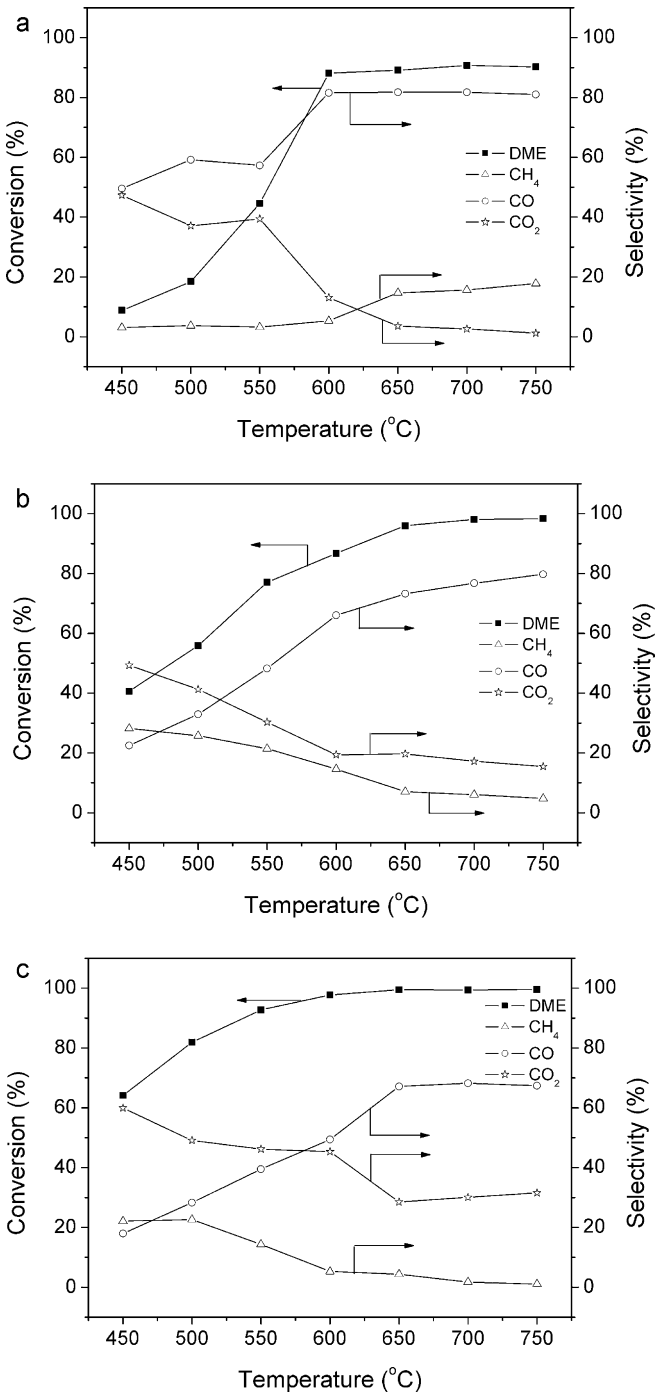

Fig. 2. DME conversion and products selectivity over the Ni + BZCY4 catalyst at various temperatures with different molar ratios of DME-to-H_2O: (a) 1:1; (b) 1:2; (c) 1:3.

DME-to-H_2O molar ratios of 1:1, 1:2 and 1:3, respectively. By introducing steam into the DME fuel gas, the DME conversion increased sharply, and a DME conversion of approximately 90% was already reached at 600 °C at DME-to-H_2O molar ratios of 1:1 and 1:2. DME conversion further increased to approximately 97% at a DME-to-H_2O molar ratio of 1:3. CH_4 is an unfavorable product from the internal steam reforming of DME because the electrocatalytic oxidation rate of CH_4 over a nickel cermet anode is relatively slow. In addition, CH_4 is believed to be the main source of coke formation over a nickel anode when operating on DME fuel [20]. Therefore, low CH_4 selectivity is preferable. Although the electrocatalytic

oxidation rate of CO over a nickel anode may also be much lower than hydrogen, the reaction of $CO + H_2O \rightarrow CO_2 + H_2$ can be easily performed at an elevated temperature over a nickel catalyst [33]. In this case, similar cell performance is typically observed for fuel cells operating on $H_2 + CO$ gas mixture and pure hydrogen; therefore, CO is an acceptable product for SOFCs operating with the internal steam reforming of DME. As expected, CH_4 selectivity was greatly reduced by introducing steam. It was almost zero at temperatures lower than 600 °C with a DME-to-H_2O molar ratio of 1:1. With a further increase in temperature, CH_4 selectivity increased slightly to reach a value of approximately 18% at 750 °C. At a DME-to-H_2O molar ratio of 1:2, a steady decrease in CO_2 and CH_4 selectivity was observed with temperature within the entire investigated range of 450–750 °C, and CH_4 selectivity was only approximately 5% at 750 °C. At a DME-to-H_2O molar ratio of 1:3, CH_4 selectivity was less than 6% even at 600 °C suggesting that the increase in the H_2O-to-DME ratio reduced CH_4 selectivity, which increased cell power output and decreased coke formation. From Fig. 2(a)–(c), it was found that the increase in the H_2O-to-DME molar ratio also resulted in an increase of CO_2 selectivity. At DME-to-H_2O ratios of 1:1, 1:2 and 1:3, the ideal reactions should be as follows, respectively:

$$CH_3OCH_3 + H_2O \rightarrow 2CO + 4H_2 \quad (1)$$

$$CH_3OCH_3 + 2H_2O \rightarrow CO + CO_2 + 5H_2 \quad (2)$$

$$CH_3OCH_3 + 3H_2O \rightarrow 2CO_2 + 6H_2 \quad (3)$$

According to Eq. (1), only CO should be detected at a DME-to-H_2O molar ratio of 1:1; however, some CH_4 and CO_2 were also formed, and the higher selectivity of CH_4 than CO_2 implies that solid carbon was less likely to be formed over the nickel cermet anode during the steam reforming process based on the carbon balance. At DME-to-H_2O molar ratios of 1:2 and 1:3, higher CO selectivity than what was expected from Eq. (2), and Eq. (3) indicates that it is likely that partial steam did not react with DME.

3.2. Carbon deposition

As demonstrated from the catalytic test, the high levels of coke formation were probably due to operating the fuel cell directly on pure DME fuel. However, the coke may be effectively suppressed by introducing steam into the fuel gas even at a low H_2O-to-DME molar ratio of 1:1. To obtain more direct information on the coke formation over the Ni + BZCY4 anode, the anode catalysts were treated in various DME + H_2O gas mixtures with different DME-to-H_2O ratios at a fixed period of 30 min. Next, the treated samples were subjected to O_2-TPO analysis. By putting the catalysts in an oxygen-containing atmosphere, with the programmatic increase in temperature, any carbon deposited over the catalyst was progressively oxidized with the production of CO_2 or CO as a result. MS analysis demonstrated that CO_2 was the main oxidation product; therefore, we only recorded the CO_2 signal. Fig. 3 shows the corresponding O_2-TPO profiles with the CO_2 signal. A large CO_2 peak was observed in the O_2-TPO profile of the catalyst after the treatment in pure DME fuel, which suggests that carbon was indeed formed over the Ni + BZCY4 catalyst. This finding agrees with the results of the catalytic test. From the O_2-TPO profile (Fig. 3). We found that the oxidation of deposited carbon began at a relatively low temperature of approximately 500 °C and ended at approximately 700 °C. It is well-known that amorphous carbon is much easier to eliminate than crystallized graphite. In a previous study, we demonstrated that the carbon from DME was mainly in an amorphous state [20], which may explain the relatively low temperature of the carbon elimination (oxidation). By introducing steam into the fuel gas, the CO_2 peak intensity decreased sharply. At DME-to-H_2O ratios of 1:2 and 1:3, almost no CO_2 peak was observed in the O_2-TPO profiles, suggesting that there were negligible amounts of coke formed over

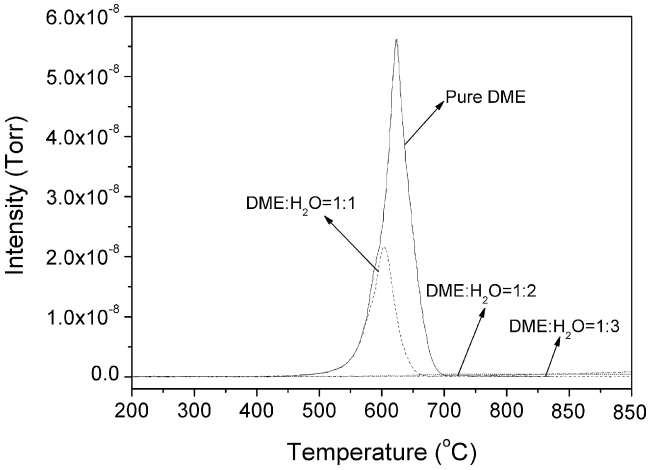

Fig. 3. O_2-TPO profiles with a CO_2 signal of Ni + BZCY4 after treatment in pure DME and various DME + H_2O gas mixtures at 700 °C for 30 min.

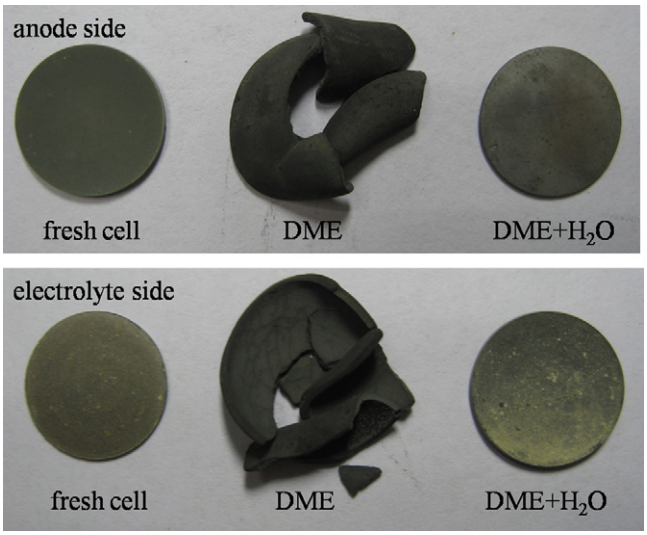

Fig. 4. Digital photos of the fresh cell and the cells after the treatment in DME or DME + H_2O (1:3) gas mixture at 700 °C for 30 min.

the Ni + BZCY4 catalysts. We believe that CH_4 was the main source for the coke formation when operating on DME fuel [20]. As shown in Fig. 2, the CH_4 selectivity was 34%, 19%, 6% and 1% when operating on pure DME, DME + H_2O (1:1), DME + H_2O (1:2) and DME + H_2O (1:3), respectively. This strongly indicates that CH_4 was likely the origin of the carbon formation.

Deposited carbon can cover the active sites of the anode and decrease the electrocatalytic activity of the electrodes. Sometimes, carbon accumulation in the electrodes may eventually destroy the geometric integrity of the electrodes and lead to the failure of the fuel cells. Two Ni + BZCY4 anode-supported BZCY4 half cells were treated in pure DME and a DME + H_2O gas mixture (DME:H_2O = 1:1) at 700 °C for 30 min. Fig. 4 shows the digital photos of the fresh cell and the cells after treatment in DME and the DME + H_2O (1:3) gas mixture. The cell after treatment in pure DME was seriously deformed, whereas the cell after treatment in the DME + H_2O gas mixture maintained its original geometric shape. This further indicates that the introduction of steam into the DME fuel gas effectively suppressed coke formation over the Ni + BZCY4 electrode.

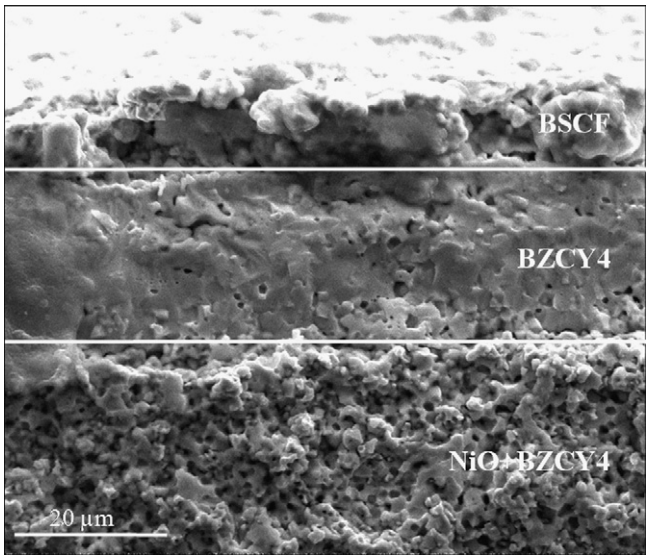

Fig. 5. Cross-sectional SEM image of the tested Ni + BZCY4|BZCY4|BSCF fuel cell.

3.3. Cell performance

Completed cells with an anode-supported thin-film BZCY4 electrolyte were fabricated using BSCF as a cathode. The thickness of the electrolytes for different cells was fixed at approximately 21 μm by precisely controlling the amount of BZCY4 powder during the dry pressing process. Fig. 5 shows a typical SEM image of the fuel cell from a cross-sectional view. The BZCY4 electrolyte was quite densified without the appearance of penetrating pinholes.

The fuel cells were first tested using 3% H_2O humidified hydrogen as the fuel. Comparable results were observed for different cells due to their similarity. Typical results at various temperatures are shown in Fig. 6(a). The open circuit voltages (OCVs) of the cell all exceeded 1.0 V suggesting a highly densified BZCY4 electrolyte layer, which agrees with the SEM observation. A peak power density of approximately 374 mW cm^{-2} was achieved at 700 °C, which was higher than our previous result of 187 mW cm^{-2} at the same temperature for a similar cell with an electrolyte thickness of ~35 μm [34]. The decrease in operating temperature resulted in a modest decrease in the cell power output, and a peak power density of approximately 192 mW cm^{-2} was reached at 500 °C. The relatively low dependence of the cell power output on the temperature can be explained in part by the fact that the protonic conductivity of BZCY4 had a low activation energy. It has been reported that the activation energy of proton diffusion is approximately 0.3–0.6 eV [35,36], which is much lower than 0.8 eV required for oxygen ion diffusion [37,38]. The linear response of the cell voltage to the polarization current suggests that the electrodes had sufficient porosity to ensure negligible concentration polarization. Fig. 6(b) and (c) shows the *I–V* and *I–P* polarization curves of two cells at different temperatures operating on pure DME fuel and a gas mixture of DME + H_2O (1:3), respectively. When operating on DME fuel, an OCV of 0.97 V was obtained at 700 °C, and peak power densities of 252, 150, 97, 39 and 8 mW cm^{-2} were reached at 700, 650, 600, 550 and 500 °C, respectively. As mentioned, hydrogen is the only electro-active fuel in proton-conducting SOFCs. Based on the catalytic test, pure DME can be decomposed to CH_4, CO_2, CO and H_2 under the catalysis of a Ni + BZCY4 cermet anode. The produced hydrogen acted as the direct fuel while CH_4, CO_2 and unconverted DME acted as the diluting gas. This indicates that the power output (252 mW cm^{-2}) and OCV (0.97 V) at 700 °C for a cell operating on pure DME were lower than those (374 mW cm^{-2} & 1.01 V) of the same cell operating on humidified hydrogen. With the decrease in operating temperature,

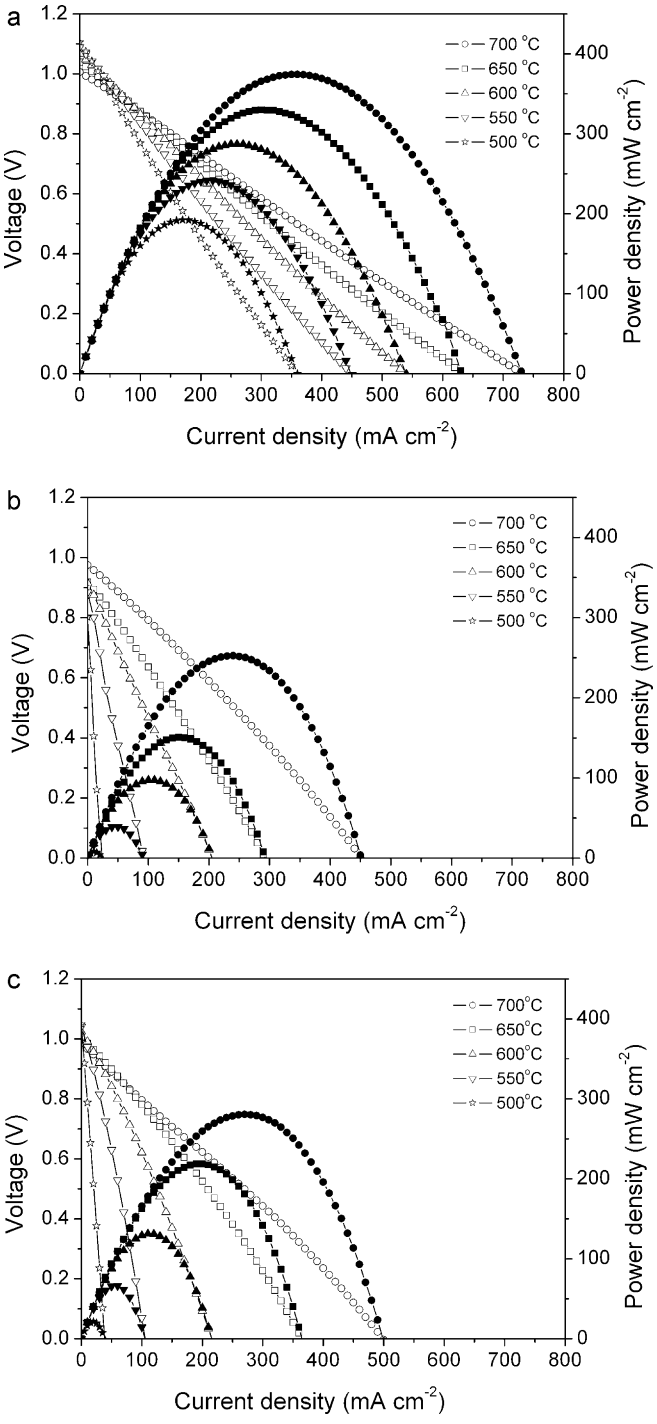

Fig. 6. Cell voltages and power densities as function of current density for fuel cells consisting of the Ni + BZCY4 anode fed with different fuels: (a) H_2; (b) pure DME; (c) DME + H_2O (1:3) gas mixture.

a slight decrease in OCV was observed, which is opposite of what occurred for hydrogen fuel. Furthermore, a sharp decrease in cell power output was observed with the decrease of temperature when operating on DME fuel, and the peak power density decreased to only 8 mW cm^{-2} at 500 °C. After operating for approximately 3 h, the fuel cell was failed due to the sudden appearance of zero OCV. When the DME + H_2O gas mixture (molar ratio of DME:H_2O = 1:3) was applied as the anode feeding gas, the cell power outputs were slightly improved. The peak power densities reached 280, 218, 131, 66 and 21 mW cm^{-2} at 700, 650, 600, 550 and 500 °C, respectively.

Table 1
Ohmic resistances (R_o) and electrode polarization resistances (R_p) of the cell at various temperatures operating on humidified hydrogen and DME+H_2O (1:3) gas mixture.

	Fuel type	700 °C	650 °C	600 °C	550 °C	500 °C
R_o (Ω cm^2)	H_2	0.68	0.74	0.85	0.99	1.19
	DME + H_2O (1:3)	0.76	0.93	1.12	1.42	1.70
R_p (Ω cm^2)	H_2	0.15	0.24	0.47	1.01	5.39
	DME + H_2O (1:3)	0.23	0.78	2.22	5.05	12.49

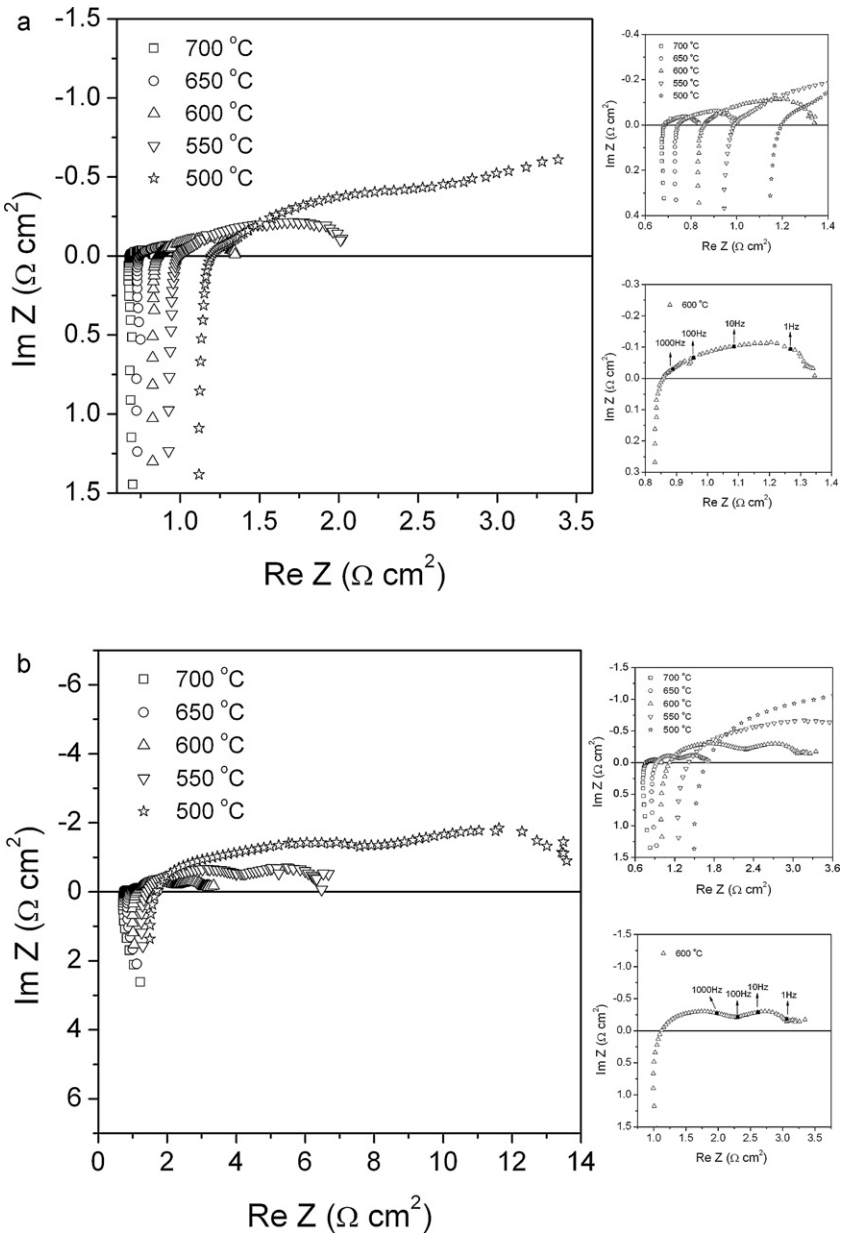

Fig. 7. Impedance spectroscopy of the fuel cell under open circuit conditions with (a) H_2 fuel and (b) DME + H_2O (1:3) gas mixture.

Unlike the cell operating on pure DME, cell performance was fairly stable when operating on DME + H_2O gas mixture. The cell OCV was slightly increased with the decrease of operating temperature and reached 0.98, 1.00, 1.02, 1.04 and 1.05 V at 700, 650, 600, 550 and 500 °C, respectively. To obtain more information to interpret the lower cell performance when operating on the DME + H_2O gas mixture than on hydrogen, the EIS of the cell operating on hydrogen and DME + H_2O gas mixture was measured under open circuit conditions, and the results are shown in Fig. 7(a) and (b). In these spectra, the intercepts at high frequencies represent the electrolyte resistances, whereas the intercepts at low frequencies represent the total resistances of the cell. The difference between the intercepts at high and low frequencies are the electrode polarization resistances, which are sum of the resistances of the two interfaces, the cathode/electrolyte resistances and the anode/electrolyte interface. The cell resistance was mainly due to the electrolyte ohmic resistance at 700 °C, and, with the decrease in operating temperature, the electrode polarization resistance increased more quickly than the electrolyte ohmic resistance. At 500 °C, the electrode polarization resistance was more than three times greater than that

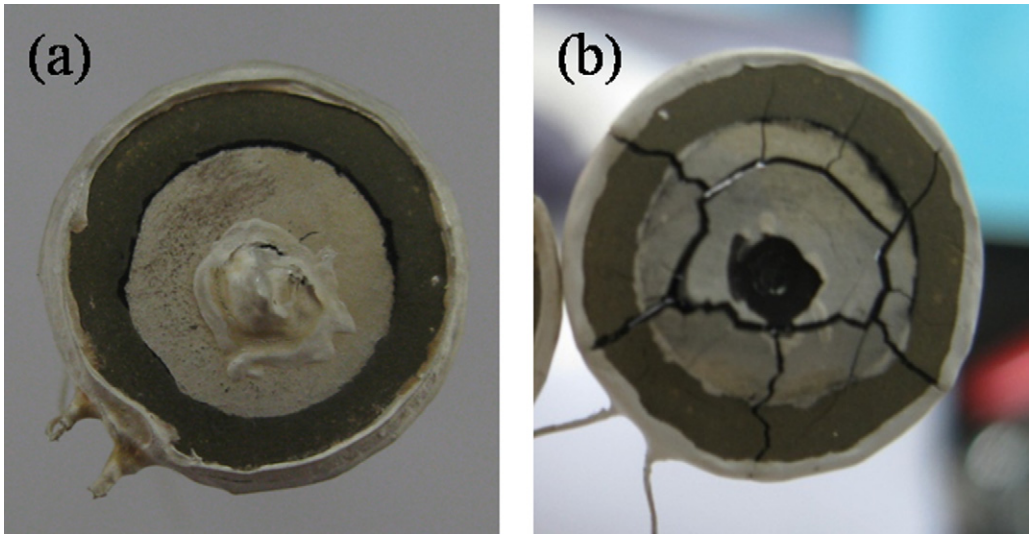

Fig. 8. Digital photos of the cells after testing with (a) DME + H_2O (1:3) mixture gas and (b) pure DME.

of the electrolyte ohmic resistance. This finding suggests that the cell power output was determined mainly by poor electrode performance at reduced temperatures, whereas the electrolyte made a significant contribution at high temperature (700 °C). When operating on the DME + H_2O gas mixture, the electrode polarization resistance increased even more quickly than when operating on hydrogen fuel with the decrease of operation temperature. Table 1 lists the ohmic resistances and electrode polarization resistances of the cell at various temperatures when operating on humidified hydrogen and the DME + H_2O (1:3) gas mixture. It was found that both the electrolyte ohmic resistance and the electrode polarization resistance for the cell operating on the DME + H_2O gas mixture were higher than those on hydrogen. The slightly larger ohmic resistance of the cell operating on the DME + H_2O gas mixture can be ascribed to the lower concentration of hydrogen in DME + H_2O mixture than that of pure hydrogen under the same flow rate. It can also be explained due to the fact that the actual temperature of the cell operating on DME + H_2O could be lower than that operating on hydrogen because the DME steam reforming is an endothermic reaction [39]. A similar lower temperature has been reported for a cell operating on ammonia compared to a cell on hydrogen [40], because ammonia decomposition is also an endothermic reaction. The electrode polarization resistance measured from a single cell is a sum of the contribution from both the anode and the cathode. Because the cathode's contribution to the electrode polarization resistance for a cell operating on a DME + H_2O gas mixture and hydrogen should be the same, the significant increase in electrode polarization resistance when operating on the DME + H_2O gas mixture must have come from the anode. It has been reported that $BaCe_{0.8}Y_{0.2}O_3$ (BCY) proton conductors are sensitive to CO_2, and high CO_2 concentrations can cause the destruction of the phase structure of BCY [41]. Although the partial substitution of Ce with Zr during the formation of BZCY4 can substantially increase the phase structure of the proton conductor against CO_2, a noticeable amount of CO_2 was still adsorbed on the surface of BZCY4 oxide under a pure CO_2 atmosphere at 650 °C for 2 h [42]. When operating on a DME + H_2O gas mixture, CO_2 was the main product from the steam reforming of DME over the anode. The *in situ* produced CO_2 can adsorb over the BZCY4 surface causing significant blocking of hydrogen surface diffusion and proton charge transfer. It is well-known that adsorption is preferred at lower temperatures; therefore, the electrode polarization resistance was sharply increased with a decrease in operating temperature. To further increase the cell power output at a reduced temperature, the selection of a proton conductor with a higher resistance to CO_2 was required. In any case, the cell still delivered an attractive power output at a temperature higher than 600 °C when operating on DME with internal steam reforming using Ni + BZCY4 as a cermet anode.

Unlike the cell operating on pure DME, which failed after testing for approximately 3 h, the performance is fairly stable for the cell operating on DME + H_2O fuel. Fig. 8(a) and (b) shows the digital photos of the cell after testing with a DME + H_2O (1:3) gas mixture and pure DME fuel from 700 to 500 °C. The cell operating on the DME + H_2O mixture gas maintained perfect integrity, whereas the cell operating on pure DME was significantly cracked, which may explain the sharp decrease in the open circuit voltage to 0 V during the measurement. This further suggests that it is of great importance to introduce steam, which increases the operation stability and the performance of a fuel cell operating on DME fuel.

4. Conclusions

This study investigated the performance of a proton-conducting SOFC with a Ni + BZCY4 cermet anode operating on DME fuel at an intermediate temperature. On the whole, the sintered Ni + BZCY4 anode catalyst exhibited acceptable catalytic activity for the decomposition and steam reforming of DME at the investigated temperature range of 500–700 °C. Carbon deposition over the Ni + BZCY4 anode surface was significant when pure DME was used as the fuel, especially at low temperatures, which led to the formation of significant cracks and caused the failure of the fuel cell during operation. By introducing steam into the DME fuel gas, carbon deposition over the anode catalyst was effectively suppressed at all investigated temperatures, and cell integrity was successfully maintained. Based on the results of the ohmic resistance and electrode polarization resistance of the cell with DME and a DME + H_2O gas mixture as fuels to improve a cell power output, the selection of a better proton-conducting phase of the anode is critical.

Acknowledgements

This work was supported by the "National Science Foundation for Distinguished Young Scholars of China" under contract No. 51025209, by "Outstanding Young Scholar Grant at Jiangsu Province" under contract No. 2008023, by program for New Century Excellent Talents (2008), and by Fok Ying Tung Education

Foundation under contract No. 111073. Prof. Shao also acknowledges the ARC future fellowship from Australia, under no. FT100100134.

References

[1] T. Hibino, A. Hashimoto, M. Yano, M. Suzuki, S. Yoshida, M. Sano, J. Electrochem. Soc. 149 (2002) A133–A136.
[2] Y. Jiang, A.V. Virkar, J. Electrochem. Soc. 148 (2001) A706–A709.
[3] Q.L. Ma, R.R. Peng, Y.J. Lin, J.F. Gao, G.Y. Meng, J. Power Sources 161 (2006) 95–98.
[4] T. Hibino, A. Hashimoto, T. Inoue, J. Tokuno, S. Yoshida, M. Sano, Science 288 (2000) 2031–2033.
[5] A.L. Dicks, J. Power Sources 61 (1996) 113–124.
[6] T. Ishihara, K. Sato, Y. Takita, J. Am. Ceram. Soc. 79 (1996) 913–919.
[7] C.R. Xia, F.L. Chen, M.L. Liu, Electrochem. Solid-State Lett. 4 (2001) A52–A54.
[8] L. Yang, C.D. Zuo, S.Z. Wang, Z. Cheng, M.L. Liu, Adv. Mater. 20 (2008) 3280–3283.
[9] E. Fabbri, S. Licoccia, E. Traversa, E.D. Wachsman, Fuel Cells 9 (2009) 128–138.
[10] Y.M. Guo, R. Ran, Z.P. Shao, S.M. Liu, Int. J. Hydrogen Energy 36 (2011) 8450–8460.
[11] H. Iwahara, T. Esaka, H. Uchida, N. Maeda, Solid State Ionics 3–4 (1981) 359–363.
[12] X.G. Zhang, S. Ohara, H. Okawa, R. Maric, T. Fukui, Solid State Ionics 139 (2001) 145–152.
[13] D. Xu, X.M. Liu, D.J. Wang, G.Y. Yi, Y. Gao, D.S. Zhang, W.H. Su, J. Alloys Compd. 429 (2007) 292–295.
[14] S.C. Singhal, Solid State Ionics 135 (2000) 305–313.
[15] Z.P. Shao, S.M. Haile, Nature 431 (2004) 170–173.
[16] S.Z. Wang, T. Ishihara, Y. Takita, Electrochem. Solid-State Lett. 5 (2002) A177–A180.
[17] P. Heo, M. Nagao, M. Sano, T. Hibino, J. Electrochem. Soc. 155 (2008) B92–B95.
[18] M. Yano, T. Kawai, K. Okamoto, M. Nagao, M. Sano, A. Tomita, T. Hibino, J. Electrochem. Soc. 154 (2007) B865–B870.
[19] E.P. Murray, S.J. Harris, H.W. Jen, J. Electrochem. Soc. 149 (2002) A1127–A1131.
[20] C. Su, R. Ran, W. Wang, Z.P. Shao, J. Power Sources 196 (2011) 1967–1974.
[21] C. Su, W. Wang, H.G. Shi, R. Ran, H.J. Park, C. Kwak, Z.P. Shao, J. Power Sources 196 (2011) 7601–7608.
[22] H. Yasutake, Y.C. Jin, K. Yamahara, M. Ihara, J. Electrochem. Soc. 157 (2010) B1370–B1375.
[23] R. Tai, K. Ui, K. Takeuchi, K. Fujimoto, S. Ito, Electrochemistry 77 (2009) 149–151.
[24] Y. Ishida, R. Tai, K. Ui, K. Takeuchi, K. Fujimoto, S. Ito, Electrochemistry 77 (2009) 225–228.
[25] W. Zhou, Z.P. Shao, R. Ran, R. Cai, Novel, Electrochem. Commun. 10 (2008) 1647–1651.
[26] G. Halasi, T. Bánsági, F. Solymosi, ChemCatChem 1 (2009) 311–317.
[27] N. Laosiripojana, S. Assabumrungrat, Appl. Catal. A 320 (2007) 105–113.
[28] N. Shimoda, K. Faungnawakij, R. Kikuchi, K. Eguchi, Int. J. Hydrogen Energy 36 (2011) 1433–1441.
[29] S. Parka, H. Kimb, B. Choib, Catal. Today 164 (2011) 240–245.
[30] S.D. Badmaev, P.V. Snytnikov, Int. J. Hydrogen Energy 33 (2008) 3026–3030.
[31] K. Faungnawakij, R. Kikuchi, T. Fukunaga, K. Eguchi, J. Phys. Chem. C 113 (2009) 18455–18458.
[32] K. Faungnawakij, R. Kikuchi, T. Matsui, T. Fukunaga, K. Eguchi, Appl. Catal. A 333 (2007) 114–121.
[33] M.M. Barroso-Quiroga, A.E. Castro-Luna, Int. J. Hydrogen Energy 35 (2010) 6052–6056.
[34] Y.M. Guo, R. Ran, Z.P. Shao, Int. J. Hydrogen Energy 36 (2011) 1683–1691.
[35] K. Katahira, Y. Kohchi, T. Shimura, H. Iwahara, Solid State Ionics 138 (2000) 91–98.
[36] K.D. Kreuer, St. Adams, W. Münch, A. Fuchs, U. Klock, J. Maier, Solid State Ionics 145 (2001) 295–306.
[37] J.D. Solier, M.A. Pérez-Jubindo, A. Dominguez-Rodriguez, A.H. Heuer, J. Am. Ceram. Soc. 72 (1989) 1500–1502.
[38] T. Hibino, A. Hashimoto, M. Suzuki, M. Sano, J. Electrochem. Soc. 149 (2002) A1503–A1508.
[39] T.A. Semelsberger, R.L. Borup, J. Power Sources 155 (2006) 340–352.
[40] Y. Lin, R. Ran, Y.M. Guo, W. Zhou, R. Cai, J. Wang, Z.P. Shao, Int. J. Hydrogen Energy 35 (2010) 2637–2642.
[41] N. Zakowsky, S. Williamson, J.T.S. Irvine, Solid State Ionics 176 (2005) 3019–3026.
[42] Y.M. Guo, Y. Lin, R. Ran, Z.P. Shao, J. Power Sources 193 (2009) 400–407.